Mobility, Power and Thermal Control of Spherex for Planetary Exploration

Article *in* Advances in the Astronautical Sciences · January 2020

2 authors:

Himangshu Kalita
The University of Arizona
53 PUBLICATIONS   **167** CITATIONS

Jekan Thangavelautham
The University of Arizona
205 PUBLICATIONS   **834** CITATIONS

Some of the authors of this publication are also working on these related projects:

Project   Automated Design of CubeSats and Small Spacecrafts View project

Project   On-Orbit Centrifuge Laboratory View project

MOBILITY, POWER AND THERMAL CONTROL OF SPHEREX FOR PLANETARY EXPLORATION

Himangshu Kalita,[*] and Jekan Thangavelautham,[†]

Some of the high priority targets outlined in the Planetary Science Decadal survey includes extreme environments of the Moon, Mars and icy moons that includes caves, canyons, pits, cliffs, skylights and craters. Exploration of these extreme and rugged environments remains out of reach from current planetary rovers and landers; however, the 2015 NASA Technology Roadmaps prioritizes the need for next-generation robotic and autonomous systems that can explore these extreme and rugged environments. We had presented an architecture of small, low-cost, modular spherical robot called SphereX that is designed to hop and roll short distances for exploring these extreme environments. The robot uses commercially off-the-shelf components for its electronics and communication. For mobility, the robot uses a H_2/O_2 propulsion system consisting of one thruster along with a 3-axis reaction wheel system to perform controlled hopping and rolling. For power, the robot uses PEM fuel cells to generate power on demand by utilizing hydrogen and oxygen. To avoid cryogenic storage, hydrogen and oxygen for the propulsion and power system is generated on demand with a water activated lithium hydride (LiH) hydrogen generator and a catalytic decomposition-based lithium perchlorate ($LiClO_4$) oxygen generator. Moreover, for the robot to survive extreme temperature ranges on the target environment, it consists of a thermal control system that relies on both active and passive thermal control elements in the form of a low emissive silver coating, a low conductive silica aerogel insulation layer, a variable emittance coating, a heat switch and an electric heater. In this paper, we present detailed control strategies for mobility, power and thermal system of SphereX for it to survive on a target environment and explore with optimal use of the chemicals.

INTRODUCTION

In the next few decades, we aspire to send human and robotic explorers to every corner of our solar system to perform orbital, surface and even subsurface exploration. These explorers will pave the way towards identifying the diverse surface environments, physical processes and structure of the planets and small bodies answering fundamental questions about the origins of the solar system, conditions to sustain life and prospects for resource utilization and off-world human settlement. Achieving this major exploration milestone remains technologically daunting but not impossible. An emerging target are the extreme environments of the Moon, Mars and icy moons, including caves, canyons, cliffs, skylights and craters. These are high-priority targets as outlined in the Planetary Science Decadal survey [1]. High resolution orbital imagery from the Lunar Reconnaissance Orbiter Camera (LROC) reveal evidence for subsurface voids and mare-pits on the lunar surface

[*] Ph.D. Candidate, Aerospace and Mechanical Engineering, University of Arizona, Tucson AZ 85721.
[†] Assistant Professor, Aerospace and Mechanical Engineering, University of Arizona, Tucson AZ 85721.

[2, 3]. Similar discoveries have been made with the HiRise camera onboard the Mars Reconnaissance Orbiter (MRO) observing the Martian surface. Exploration of these extreme and rugged environments remains out of reach from current planetary rovers and landers; however, the 2015 NASA Technology Roadmaps prioritizes the need for next-generation robotic and autonomous systems that can explore these extreme and rugged environment [4]. The challenges are three-fold and stem from current landing technology that requires wide-open spaces with no obstacles or landing hazards. A second challenge stems from current planetary vehicle architectures. Planetary rovers and landers ever since Luna 9, the first mission to soft-land on the Moon, have been generally growing in size and capability to house a growing variety of sophisticated science instruments. A third challenge has been the high standards of mission assurance expected. Due to the high costs and prestige for the nations involved, any form of exploratory risk that may reduce the life of the mission or result in damage to one or more subsystems is avoided. This is despite the potential science rewards from taking these exploratory risks.

A credible solution is to develop an architecture that permits taking high exploratory risks that translates into high reward science but without compromising the rest of the mission. Rapid advancement in electronics, sensors, actuators and power supplies have resulted in ever-shrinking devices and instruments that can be housed in small platforms. This has resulted in the wide adoption of CubeSats for Low Earth Orbit (LEO) missions and technology demonstrations. CubeSats are emerging as platform for performing high-risk, high-reward interplanetary exploration [5]. The technology uses Commercial-Off-The-Shelf (COTS) technology with adaptations to the space environment. Further technological advancement is leading towards radiation hardened version of these components for use in deep-space and planetary environments. However, these technologies still need to be proven in these planetary environments.

We present an architecture of small, low-cost, modular spherical robot called SphereX that is designed for exploring extreme environments like caves, lava tubes, pits and canyons in low-gravity environments like the Moon, Mars, icy moons and asteroids through hopping and rolling. In this paper, we present detailed control strategies for mobility, power and thermal system of SphereX for it to survive on a target environment and explore with optimal use of the chemicals. For mobility control, we developed an optimal attitude and thrust controller for the robot to reach a desired target by hopping and rolling using minimum fuel and power. Power is provided with fuel cells, but in order to avoid voltage oscillations that reduces the life of the fuel cell, we have adapted a fuel cell-battery hybrid power control system that can handle varying power demands for the robot. For thermal control, the robot efficiently uses the heat generated internally along with the variable emittance coating, heat switch and electric heater to survive through the desired lifetime. Using this method of combined mobility, power and thermal control system, the robot will be able to explore more than 1000 meters and survive for ~15 days on the surface of the Moon.
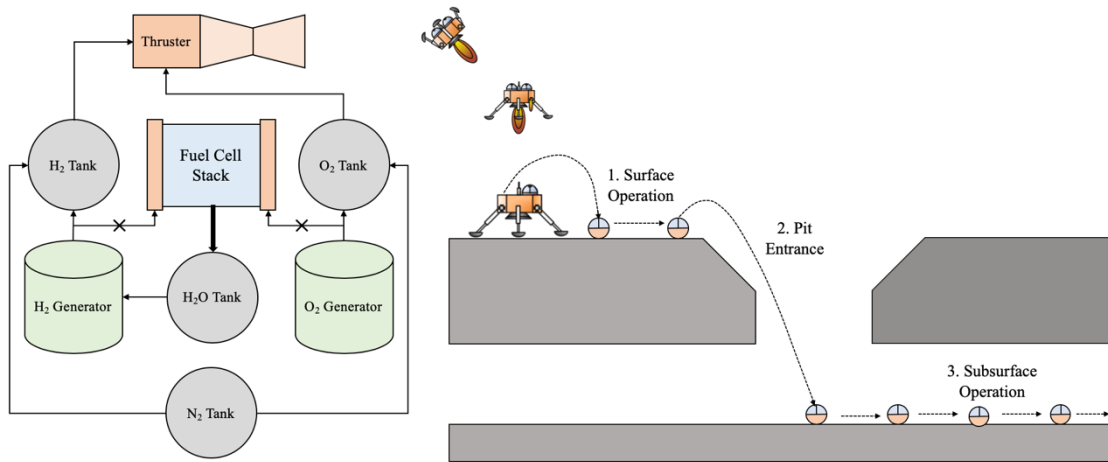
SPHEREX

SphereX is a small, low-cost, modular spherical robot that is designed to hop and roll short distances for exploration as shown in Figure 1 [6-11]. It consists of space grade electronics like computer board for command and data handling, power board for power management and radio transceiver with multiple S/X-band antennas for communicating among multiple robots. Mobility is achieved through the combined action of a propulsion system consisting of one thruster along with an attitude control system consisting of 3 reaction wheels to perform controlled ballistic hopping. The 3-axis reaction wheel system can also be used for controlled rolling mobility. Moreover, it consists of a power system for power generation, storage and distribution among all the subsystems and a thermal system comprising of several active and passive elements to maintain its desired body temperature for survival. The rest of the volume is accompanied by payloads in the form of a

pair of stereo cameras for imaging and a LiDAR system for mapping and navigation. A large rover or lander may carry several of these SphereX robots that can be tactically deployed to explore and access extreme environments inaccessible by it.
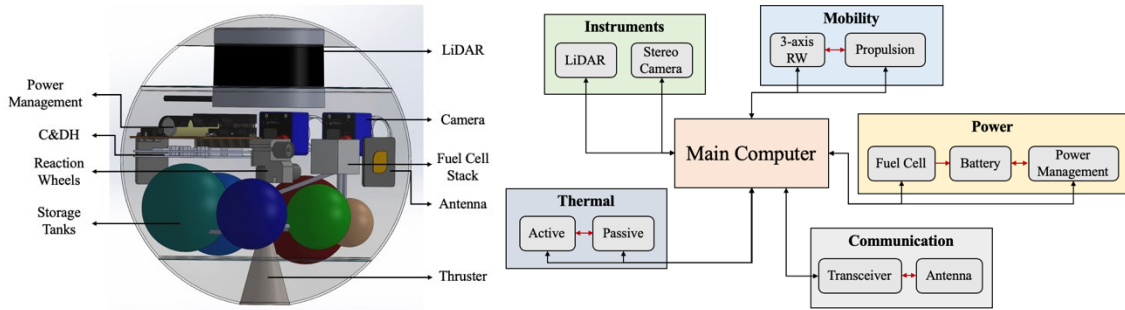
Figure 1: (Left) Internal view of the major components of SphereX, (Right) Hardware architecture of SphereX with major subsystems.

Figure 2: (Left) Schematic of the combined power and propulsion system of SphereX using PEM fuel cells and H_2/O_2 propulsion. (Right) A conceptual mission scenario for exploring planetary pits/lava tubes using SphereX.

The power system for SphereX is in the form of PEM fuel cells and the propulsion system is a H_2/O_2 propulsion system. The system consists of a water activated lithium hydride (LiH) hydrogen generator and a catalytic decomposition-based lithium perchlorate ($LiClO_4$) oxygen generator as shown in Figure 2(Left). The hydrogen and oxygen are fed into the fuel cell system with the help of micropumps while it is fed into the combustion chamber with the help of pressurized nitrogen gas. The water tank carries water for the hydrogen generator which is again fed with a micropump. It also stores the water produced by the PEM fuel cell during its operation. The PEM fuel cell power supply is implemented as a fuel cell-battery hybrid system to maximize its life. Figure 2(Right) shows a conceptual mission scenario for exploring planetary pits/lava tubes. A lander carrying multiple SphereX robots would descent nearby a pit/lava tube and deploy the robots one by one. Each robot will have three phases 1. Surface operation to approach the pit entrance, 2. Pit entrance maneuver, and 3. Sub-surface operation to explore the pit [13].

MOBILITY SYSTEM

Mobility of SphereX is achieved with the help of a miniaturized propulsion system and a 3-axis reaction wheel system. The combined action of the propulsion and the reaction wheel system is used for ballistic hopping mobility and the reaction wheel system alone is used for rolling mobility.

Ballistic Hopping Mobility

Two modes of ballistic hopping are identified for the robot to be able to explore extreme environments: a) Hard-landing mode for exploring short distances, and b) Soft-landing mode for pit entrance and exploring long distances whose time diagrams are shown in Figure 3.
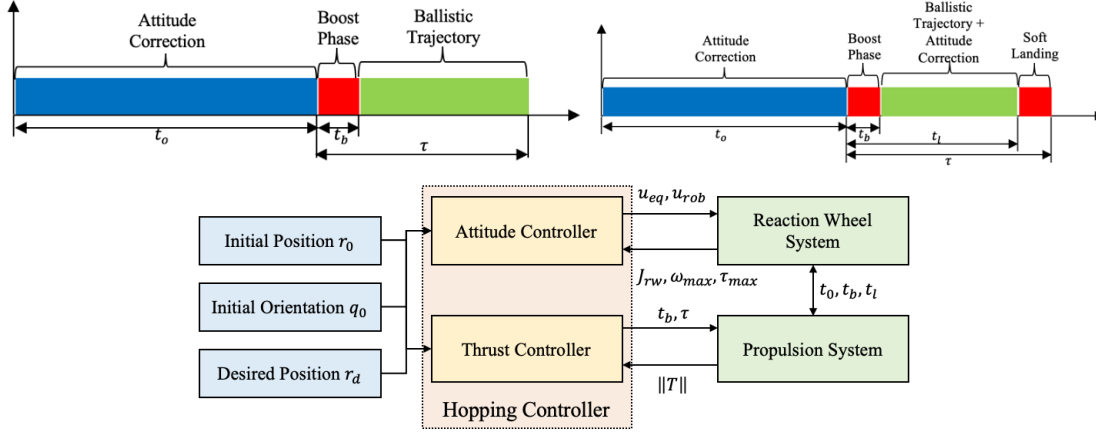
Figure 3: (Top-Left) Time diagram of hard-landing hopping mode, (Top-Right) Time diagram of soft-landing hopping mode, (Bottom) Control system architecture for ballistic hopping.

The control system for ballistic hopping consists of an *attitude controller* and a *thrust controller* as shown in Figure 3(Bottom). The 3-axis reaction wheel system is used for maintaining roll, pitch, and yaw angles along its principal axes while the propulsion system providing the desired thrust to execute a ballistic hop. During this mode of ballistic hopping the robot needs to reach a desired position $r_d = (x_d, y_d, z_d)$ from its initial position $r_0 = (x_0, y_0, z_0)$. During the attitude correction phase, the robot needs to orient itself from its initial attitude states $q_0 = (\phi_0, \theta_0, \psi_0)$ to the desired attitude states $q_d = (\phi_d, \theta_d, \psi_d)$ while on ground such that the thruster is oriented in the desired direction. For the attitude correction phase a sliding-mode attitude controller is designed to maintain its desired attitude states.

Attitude Controller: The attitude dynamics of the robot actuated by a set of 3 reaction wheels are described by Equation (1).

$$\dot{\omega}_s = -J_s^{-1}\widetilde{\omega}_s(J_s\omega_s + h_{rw}) + J_s^{-1}(\tau_{rw} + \tau_{ext}) \tag{1}$$

where, ω_s is the angular velocity of the robot in its body fixed frame ($\mathcal{B}$), $\widetilde{\omega}_s$ is the cross-product matrix of ω_s, J_s is the robot's inertia matrix, h_{rw} is the net reaction wheel angular momentum, τ_{rw} is the net reaction wheel torque, and τ_{ext} is the external torque. The dynamics are second order and can be written as: $\dot{\omega}_s = f + Bu$, where $f = -J_s^{-1}\widetilde{\omega}_s(J_s\omega_s + h_{rw}) + J_s^{-1}\tau_{ext}$ is the drift function, $B = J_s^{-1}E_{rw}$ is the input matrix, and $u = \tau_{ext}$ is the control input. The robot's attitude is represented by the Modified Rodrigues Parameters (MRP), σ. Now, let's define the sliding variable (s) as in Equation (2).

$$s(\delta\omega, \delta\sigma) = \delta\omega + \Lambda\delta\sigma + \Lambda_I \int_0^t \delta\sigma dt \tag{2}$$

where, Λ and Λ_I are the control gains which are 3x3 symmetric positive-definite constant matrices, $\delta\omega = \omega_s - {}^{\mathcal{BR}}R^{\mathcal{R}}\omega_d$ is the difference in angular velocity of the robot and the desired angular velocity with ${}^{\mathcal{BR}}R$ as the rotation matrix from the reference frame ($\mathcal{R}$) to the body frame ($\mathcal{B}$), and $\delta\sigma = \sigma - \sigma_d$ is the difference between the robot's MRP vector and desired MRP vector. The control gains are selected based on the desired system response by selecting the damping ratio ξ and the time, T it takes for the state errors to decay to $1/e$ based on the initial values such that, $\xi = \Lambda/(4\sqrt{\Lambda_I})$ and $T = 8/\Lambda$. Based on the system let us consider the Lyapunov function as:

$$V(\delta\sigma) = 2\log(1 + \delta\sigma^T\delta\sigma) + \frac{1}{2}\left(\Lambda_I \int_0^t \delta\sigma dt\right)^T \Lambda_I^{-1}\left(\Lambda_I \int_0^t \delta\sigma dt\right) \tag{3}$$

The function $V(\delta\sigma)$ is continuously differentiable, $V(\delta\sigma = 0) = 0$, and $V(\delta\sigma \neq 0) > 0$ and its derivative $\dot{V}(\delta\sigma) = -\delta\sigma^T\Lambda\delta\sigma$ is negative semi-definite, thus the system is Lyapunov stable. The continuous control law (u_{eq}) is designed such that the sliding manifold is reached and sliding occurs on the manifold which results in $\dot{s}(\delta\omega, \delta\sigma) = 0$. By solving for $\dot{s}(\delta\omega, \delta\sigma) = 0$, we derive the equivalent control expression u_{eq} as:

$$u_{eq} = B^{-1}\left(-f + {}^{\mathcal{BR}}R^{\mathcal{R}}\dot{\omega}_d - \tilde{\omega}_s {}^{\mathcal{BR}}R^{\mathcal{R}}\omega_d - \frac{1}{4}\Lambda B(\delta\sigma)\delta\omega - \Lambda_I\delta\sigma\right) \tag{4}$$

However, to address the condition where the sliding variable (s) is not on the sliding surface, a robustness term (u_{rob}) is added that guarantees that s converges to the sliding surface. The robust control term u_{rob} is expressed as:

$$u_{rob} = B^{-1}K sign\big(s(\delta\omega, \delta\sigma)\big) \tag{5}$$

where, K is a diagonal matrix. The final control law includes the equivalent and robust control terms as $u = u_{eq} - u_{rob}$.

Thrust Controller: During the boost phase, the thruster provides a constant thrust $\|\mathbb{T}\|$ for time t_b with the attitude control system maintaining the desired attitude states $q_d = (\phi_d, \theta_d, \psi_d)$. For the soft-landing mode, the robot has an additional soft-landing phase during which the thruster provides the same constant thrust $\|\mathbb{T}\|$ for time $(\tau - t_l)$ such that the robot lands at zero velocity. The dynamic equations governing the motion of the robot in the reference frame ($\mathcal{R}$) can be expressed as Equation (6).

$$\dot{r} = v, \quad \dot{v} = \begin{cases} g + \dfrac{\mathbb{T}}{m} & if\ t < t_b \\ g & if\ t_b < t < t_l, \\ g + \dfrac{\mathbb{T}}{m} & if\ t_l < t < \tau \end{cases} \quad \dot{m} = \begin{cases} -\dfrac{\|\mathbb{T}\|}{I_{sp}g_0} & if\ t < t_b \\ 0 & if\ t_b < t < t_l \\ -\dfrac{\|\mathbb{T}\|}{I_{sp}g_0} & if\ t_l < t < \tau \end{cases} \tag{6}$$

where, $\mathbb{T}$ is the thrust in the reference frame denoted by $\mathbb{T} = {}^{\mathcal{RB}}R\|\mathbb{T}\|$, with ${}^{\mathcal{RB}}R$ being the rotation matrix from the body frame ($\mathcal{B}$) to the reference frame ($\mathcal{R}$). To solve for t_b, t_l and τ, we apply an optimal control theory approach where the objective is to minimize the total fuel consumption. Four constraints are added, with the design variables are $\mathbb{d} = [t_b, t_l, \tau]$ and the optimization problem is mathematically expressed as Equation (7).

$$\min f(\mathbb{d}) = \int_0^{t_b} \|\mathbb{T}\| \, dt + \int_{t_l}^{\tau} \|\mathbb{T}\| \, dt$$

$$subject\ to \begin{cases} g_1(\mathbb{d}) \equiv t_b - t_l < 0 \\ g_2(\mathbb{d}) \equiv t_l - \tau < 0 \\ g_3(\mathbb{d}) \equiv \|r(\tau) - r_d\|^2 = 0 \\ g_4(\mathbb{d}) \equiv \|v_\tau\|^2 = 0 \end{cases} \tag{7}$$

The same dynamics equations and optimization problem are used for both the hard-landing and soft-landing mode except for during the hard landing mode $t_l - \tau = 0$, and the fourth constraint is ignored.

Rolling Mobility

For rolling control, the robot needs to reach a desired position $r_d = (x_d, y_d)$ from its initial position $r_0 = (x_0, y_0)$. By imposing the no slip constraints, the linear velocity of the robot is computed as, $v = {}^{\mathcal{R}}\omega \times r e_3$, where ${}^{\mathcal{R}}\omega$ is the angular velocity of the robot in the reference frame. The objective is to stabilize the states $r = (x, y) \in \mathbb{R}^2$ to the desired equilibrium states $r_d = (x_d, y_d)$. We use a control law for this objective to determine the desired angular velocities ${}^{\mathcal{R}}\omega_d$ in the reference frame ($\mathcal{R}$) as in Equation (8).

$$^{\mathcal{R}}\omega_d = \left(\frac{k}{r}(y - y_d), \quad -\frac{k}{r}(x - x_d), \quad 0 \right) \tag{8}$$

where $k > 0$ are free and is a linear state-feedback control law but when transformed into body coordinate velocities ω_s, it is nonlinear. The closed-loop system with this control law is globally exponentially stable with respect to $e_{xy} = (x - x_d, y - y_d)$ and $k > 0$. Considering the Lyapunov function $V: \mathbb{R}^2 \to \mathbb{R}$ defined by $V = (1/2)e_{xy}^T e_{xy} > 0$ which is a positive definite function, the derivative of V along the trajectories of the closed loop system is, $\dot{V} = -k e_{xy}^T e_{xy} = -2kV < 0$. Thus, the closed-loop system is globally exponentially stable. Now, with the desired angular velocities determined, we use the sliding-mode controller-based attitude controller discussed above to control the reaction wheels to reach the desired equilibrium states.

Monte-Carlo Simulations

To evaluate the performance of the controllers used for SphereX, a Monte Carlo simulation was performed with 250 numerical simulations with various input parameter combinations. The constants that vary between each simulation are the initial conditions (angular position, angular velocity) of the robot, inertia matrix terms, reaction wheel spin axis inertia, reaction wheel spin axis (defined by $\theta_1, \theta_2, \theta_3$), external torque, and magnitude of thrust. The nominal values of each constant and their distribution are shown in Table 1 for SphereX with mass $m = 3$kg, radius $r = 13$cm, reaction wheel inertia $J_{rw} = 2.65e^{-5}$kg-m^2 and gravity $g = 1.62$m/s^2.

Table 1: Nominal values and distribution used for the Monte Carlo Simulations

| Variable	Nominal Value	Distribution
ϕ, θ, ψ	0.0	Uniform (± 0.5)
$\omega_{s1}, \omega_{s2}, \omega_{s3}$	0.0 rad/s	Uniform (± 0.75 rad/s)
$J_{s(11)}, J_{s(22)}, J_{s(33)}$	$2mr^2/5$ kg-m^2	Normal ($\sigma = 10\%$)
$J_{s(12)}, J_{s(13)}, J_{s(23)}$	0.0 kg-m^2	Normal ($\sigma = 0.001$ kg-m^2)

| $J_{rw(1)}, J_{rw(2)}, J_{rw(3)}$	J_{rw} kg-m^2	Normal ($\sigma = 10\%$)
$\theta_{2(1)}, \theta_{3(1)}, \theta_{1(2)}, \theta_{3(2)}, \theta_{1(3)}, \theta_{2(3)}$	0.0 rad	Normal ($\sigma = 0.0175$ rad)
τ_{ext}	0.01 N-m	Uniform (± 0.0035)
$\|\mathbb{T}\|$	$2mg$ N	Normal ($\sigma = 10\%$)
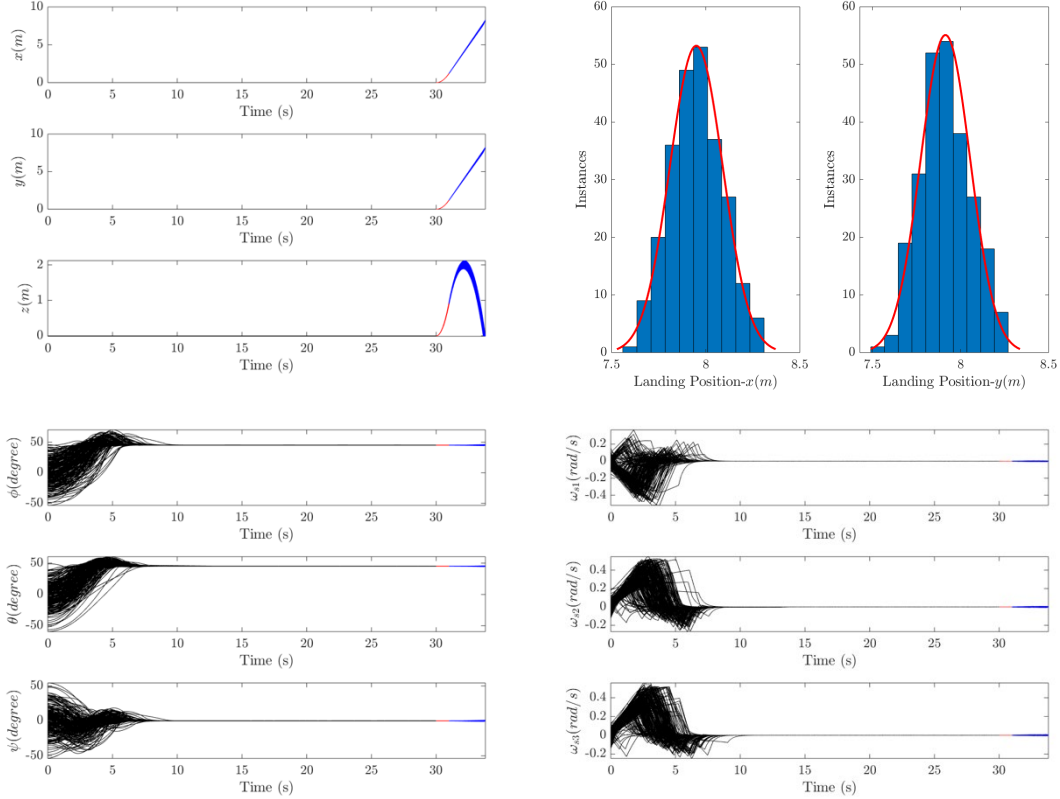
Figure 4: Monte Carlo time history of (Top-Left) Position of the robot when commanded to hop from its initial position $r_0 = (0, 0, 0)$ to its desired position $r_d = (8, 8, 0)$. (Top-Right) Histogram of the landing position of the robot fitted to a gaussian distribution. (Bottom-Left) Euler angles of the robot in 'ZYX' Euler angle notation. (Bottom-Right) Angular velocities of the robot in the body fixed frame.

Figure 4 shows the Monte Carlo time history of the position, Euler angles, and angular velocities in the body fixed frame along with the histogram of the landing position of the robot when commanded to hop from its initial position $r_0 = (0,0,0)$ to its desired position $r_d = (8,8,0)$. It can be seen that the mean of the landing position of the robot along x and y-axis are 7.95 and 7.91 m and the standard deviations are 0.145 and 0.146 m. Figure 5 shows the Monte Carlo time history of the position and velocity in x, z-axis, Euler angles, and angular velocities in the body fixed frame of the robot when commanded to perform a soft-landing hop from its initial position $r_0 = (0,0,0)$ to its desired position $r_d = (55,0,-100)$ to enter the pit. Figure 6 shows the Monte Carlo time history of the position, and angular velocities in the body fixed frame of the robot when commanded to roll from its initial position $r_0 = (0,0)$ to its desired position $r_d = (1,-1)$.
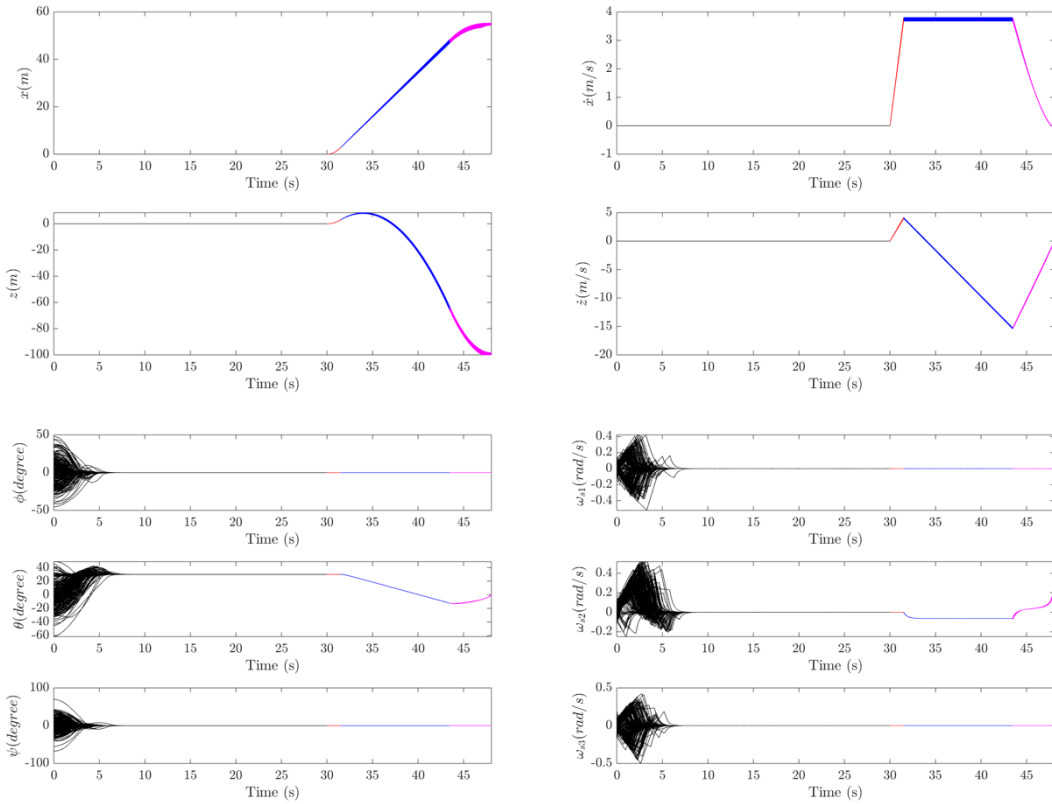
Figure 5: Monte Carlo time history of (Top-Left) Position of the robot in x and z-axis when commanded to perform a soft-landing hop from its initial position $r_0 = (0, 0, 0)$ to its desired position $r_d = (55, 0, -100)$. (Top-Right) Velocity of the robot in x and z-axis. (Bottom-Left) Euler angles of the robot in 'ZYX' Euler angle notation. (Bottom-Right) Angular velocities of the robot in the body fixed frame.
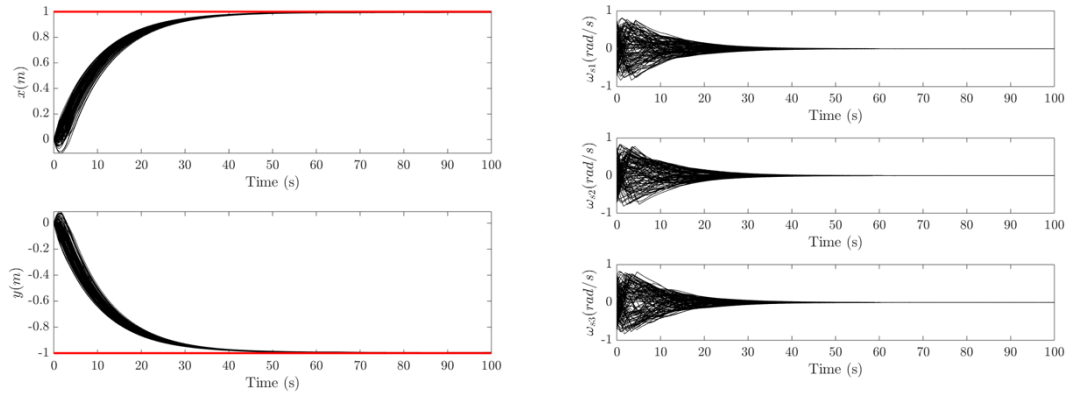
Figure 6: Monte Carlo time history of (Left) Position of the robot along x and y-axis when commanded to roll from its initial position $r_0 = (0, 0)$ to its desired position $r_d = (1, -1)$. (Right) Angular velocities of the robot in the body fixed frame.

POWER SYSTEM

The power system consists of a stack of PEM fuel cells where power is generated on demand. Each fuel cell consists of a negatively charged electrode (anode), a positively charged electrode (cathode), and an electrolyte membrane. Hydrogen is oxidized on the anode and oxygen is reduced on the cathode. Protons are transported from the anode to the cathode through the electrolyte membrane, and the electrons are carried to the cathode over the external circuit. The fuel cell layers are the PEM, gas diffusion layer (GDL) and catalyst layers as shown in Figure 7 (Left) [12]. For a power demand P, each cell operating at a voltage V, the rate of oxygen and hydrogen used are expressed as Equation (9).

$$\dot{O}_2 = 8.29 \times 10^{-8} \frac{P}{V} \frac{\text{kg}}{\text{s}}, \quad \dot{H}_2 = 1.05 \times 10^{-8} \frac{P}{V} \frac{\text{kg}}{\text{s}} \tag{9}$$

In a PEM fuel cell, water is produced as a byproduct and the rate of water generated is given by Equation (10).

$$\dot{H_2O} = 9.34 \times 10^{-8} \frac{P}{V} \frac{\text{kg}}{\text{s}} \tag{10}$$

The hydrogen and oxygen required for the operation of the fuel cell are produced on demand by the hydrolysis of LiH and catalytic thermal decomposition of LiClO4. The water produced as a byproduct of the operation of the fuel cell will be stored in the water tank for hydrolysis of LiH. Moreover, the operating voltage of a PEM fuel cell is less than the theoretical value due to losses or irreversibilities in the form of activation losses, fuel crossover and internal currents, ohmic losses and mass transport or concentration losses [12]. Adding all these losses, the operating voltage of a fuel cell at a current density i can be expressed as Equation (11).

$$V = E_{oc} - ir - A \ln(i) + m e^{(ni)} \tag{11}$$

Where, E_{oc} is the open circuit voltage, r is the area-specific resistance, A is a constant denoting the slope of the Tafel line for the particular fuel cell, and m and n are constants for mass-transfer losses. Thus, for the design of the fuel cell system, the goal is to find the optimal number of fuel cells and current density such that it can operate at a constant power demand P for a mission lifetime Γ. However, the different subsystems of SphereX operates at different cycles and as such there is a varying power demand. A varying load connected directly to fuel cell would cause voltage oscillations that reduce the life of the fuel cell. Hence the power system of SphereX consists of a fuel cell-battery hybrid system. The fuel cell constantly charges the battery at constant power, and the battery along with a power management board handles the high and varying demands of the load as shown in Figure 4 (Bottom-Left).
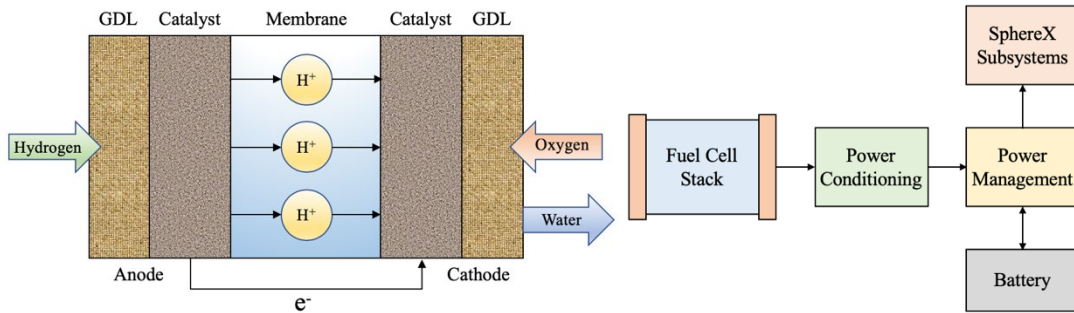
Figure 7: (Left) A PEM fuel cell and its major components, (Right) Fuel cell-battery hybrid system for power management.

THERMAL SYSTEM

In order to prevent the robot from freezing and overheating without compromising mechanical and thermal reliability and stability, we implement a thermal control architecture that relies on both active and passive thermal control elements. The proposed thermal control architecture relies on a low emissive silver coating finish and a low conductive silica aerogel insulation layer along with thermal control heat rejection/generation mechanism composed of a variable emittance coating, a heat switch and an electric heater. Figure 8 shows the thermal model of the robot with all heat transfer modes.
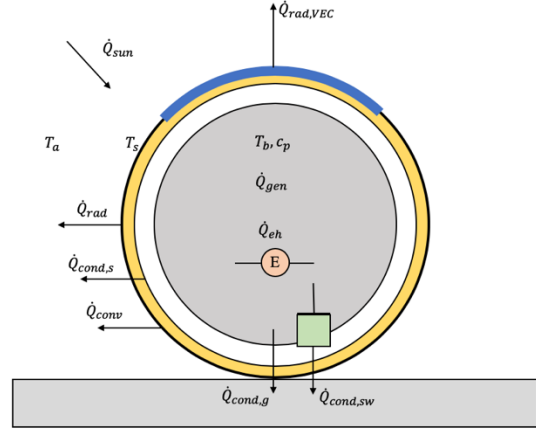
Figure 8: Modes of heat transfer involved.

The model consists of a spherical shell of mass m_s and specific heat $c_{p,s}$, representing the robot shape, with a low outer emissivity coating (ϵ_s) and a thick inner insulation layer with conductivity (λ_{in}). The temperature of the outer shell is represented as T_s, and that of the surrounding as T_a. All the internal components of the robot are assumed to be a homogeneous spherical body with temperature T_b, mass m_b and specific heat $c_{p,b}$. Considering only half of the robot surface is exposed to incoming solar radiation, the amount of absorbed irradiation by the robot is expressed as:

$$\dot{Q}_{sun} = \epsilon_s \frac{A_s}{2} \sigma \left(\frac{r_s}{r}\right)^2 T_{sun}^4 \tag{12}$$

where, A_s is the shell surface area, σ is the Stefan-Boltzmann constant, r_s is the radius of the sun, r is the distance from the sun, and T_{sun} is the black body temperature of the sun. Heat radiation also plays a major role due to frequent absence of atmosphere, and heat radiation of a sphere in a large enclosure is modeled as $\dot{Q}_{rad} = \sigma \epsilon_s A_s (T_s^4 - T_a^4)$. However, in the presence of a variable emittance coating (VEC), the apparent surface emissivity $\epsilon_{s,vec}$ influences the robot radiative heat loss and can be expressed as:

$$\dot{Q}_{rad,[vec]} = \sigma \left[\epsilon_s \left(1 - \frac{A_{vec}}{A_s}\right) + \epsilon_{s,vec} \frac{A_{vec}}{A_s}\right] A_s (T_s^4 - T_a^4) \tag{13}$$

where, A_{vec} is the VEC surface area. Conduction through the insulation layer of the robot is described as:

$$\dot{Q}_{cond,s} = \frac{4\pi \lambda_{in}(T_b - T_s)}{\dfrac{1}{\left(\dfrac{D}{2} - x\right)} - \dfrac{1}{\dfrac{D}{2}}} \tag{14}$$

where, x is the insulation layer thickness, and D is the diameter of the insulation layer. Heat loss into the ground is described as:

$$\dot{Q}_{cond,g} = \lambda_{in} A_{cont} \frac{T_b - T_a}{x} \tag{15}$$

where, A_{cont} is the contact area of the robot and the ground. Heat convection is determined by the following equation, if it plays a role in heat transfer

$$\dot{Q}_{conv} = hA_s(T_s - T_a) \tag{16}$$

where, h is the heat transfer coefficient. Moreover, a heat switch is implemented to reject excess heat from the robot's interior into the surrounding atmosphere by shunting the silica aerogel insulation layer when needed. The heat released is determined as:

$$\dot{Q}_{cond,sw} = \lambda_{sw} A_{sw} \frac{T_b - T_a}{x_{sw}} \tag{17}$$

where, λ_{sw} is the thermal conductivity of the switch, A_{sw} is the switch contact area, and x_{sw} is the switch length. In addition, an electric heater is implemented to heat the robot's interior to a desired temperature $T_{b(des)}$ if needed, and the heat required is modeled as:

$$Q_{eh} = m_b c_{p,b}(T_{b(des)} - T_b) \tag{18}$$

Moreover, heat is generated during the operation of the robot by different subsystems (mobility (propulsion), power (fuel cell), communication) which is denoted by $\dot{Q}_{gen}$. As such we implement the thermal model with two state variables T_b and T_s and the differential equations governing them is shown as:

$$
\begin{aligned}
m_b c_{p,b} \dot{T}_b &= \dot{Q}_{gen} - \dot{Q}_{cond,s} - \dot{Q}_{cond,g} - \dot{Q}_{cond,sw} + \dot{Q}_{eh} \\
m_s c_{p,s} \dot{T}_s &= \dot{Q}_{sun} + \dot{Q}_{cond,s} - \dot{Q}_{rad,[vec]} - \dot{Q}_{conv}
\end{aligned}
\tag{19}
$$

Thermal Control System: With the mathematical model of the thermal system defined, we implement a thermal control system such that the body temperature is maintained at a constant desired temperature $T_{b(des)}$. The control variables are $\epsilon_{s,vec}$, $\dot{Q}_{cond,sw}$ and Q_{eh} which are controlled according to Equation (20).

$$
\begin{aligned}
\dot{\epsilon}_{s,vec} &= k_1 (T_{b(des)} - T_b) \\
\dot{Q}_{cond,sw} &= \begin{cases} \lambda_{sw} A_{sw} \dfrac{T_b - T_a}{x_{sw}} & if\ T_{b(des)} > T_b \\ 0 & otherwise \end{cases} \\
Q_{eh} &= \begin{cases} k_2 m_b c_{p,b}(T_{b(des)} - T_b) & if\ T_{b(des)} < T_b \\ 0 & otherwise \end{cases}
\end{aligned}
\tag{20}
$$
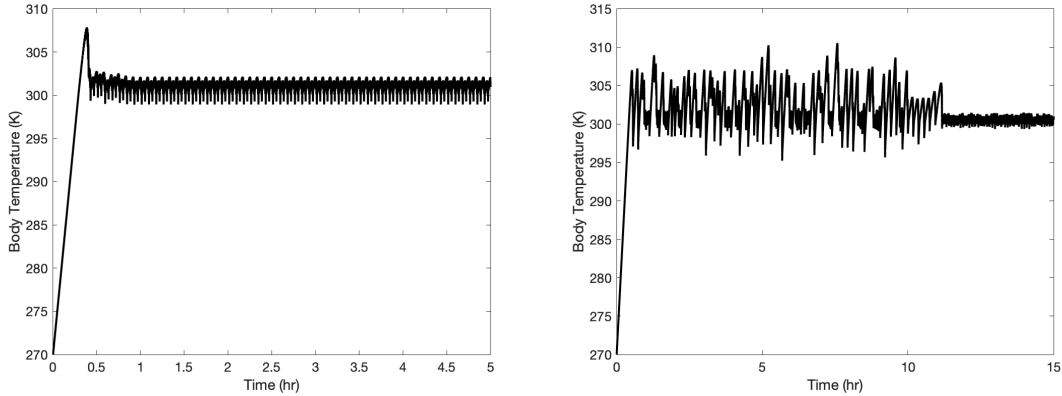
Figure 9: Body temperature of the robot for (Left) Test Scenario 1: surface exploration on Mare Tranquilitatis for 5 hours, (Right) Test Scenario 2: sub-surface exploration of Mare Tranquilitatis pit for 15 hours.

We ran two simulations for the thermal control system: *Test Scenario 1* – Surface exploration of Mare Tranquilitatis on Moon for 5 hours with ambient temperature $T_a = 340K$ and desired temperature $T_{b(des)} = 300\ K$ and *Test Scenario 2* – Sub-surface exploration of Mare Tranquilitatis pit on Moon that consists of surface exploration for 10 hours with ambient temperature $T_a = 340K$ and pit exploration for 5 hours with ambient temperature $T_a = 250K$ and desired temperature $T_{b(des)} = 300\ K$. Figure 9(Left) shows the body temperature of the robot for Test Scenario 1 and Figure 9(Right) shows the body temperature for Test Scenario 2. It can be seen that the robot was able to maintain its body temperature of 300 K with a standard deviation less than 10 K.

CONCLUSION

This paper presented the SphereX robot that uses a miniaturized H_2/O_2 propulsion system along with a 3-axis reaction wheel system to perform controlled ballistic hopping and rolling for exploring extreme off-world environments like caves, pits and lava tubes on the surface of the Moon and Mars. However, for exploring pits and caves on the surface of the Moon and Mars, the hardest challenge is to enter through the pit/lava tube entrance as the distance from the entrance to the floor are ~100 meters. As such, SphereX is equipped with two modes of hopping mobility: soft-landing and hard-landing mode. The soft-landing mode will be used to enter the pits and lava tubes so that the robot can land on the floor of the entrance at approximately zero velocity. It can also be used to traverse large distances when needed. Comparatively, the hard-landing mode is much more efficient in terms of fuel use and will be used to traverse shorter distances in the order of 10 meters. Moreover, the 3-axis reaction wheel system can also be used for rolling mobility when needed. For power, the robot will use PEM fuel cells to produce power on demand using a fuel cell-battery hybrid system. To avoid cryogenic storage of hydrogen and oxygen for the fuel cell and the propulsion system, hydrogen is generated through the hydrolysis reaction of lithium hydride and oxygen is generated through thermal decomposition reaction of lithium perchlorate. The paper also presented a thermal control system for SphereX that uses a combination of active and passive thermal elements to maintain its body temperature within a desired temperature for survival. Using this method of combined mobility, power and thermal control system, the robot will be able to explore more than 1000 meters and survive for ~15 days on the surface of the Moon.

ACKNOWLEDGMENTS

REFERENCES

[1] National Academies of Sciences, Engineering, and Medicine. 2011. Vision and Voyages for Planetary Science in the Decade 2013-2022. Washington, DC: *The National Academies Press*. doi: 10.17226/13117.

[2] R.V. Wagner and M.S. Robinson, "Distribution, formation mechanisms, and significance of lunar pits," *Icarus*, Vol. 237, pp. 52-60, 2014.

[3] M.S. Robinson et al., "Lunar reconnaissance orbiter camera (LROC) instrument overview," *Space Science Reviews*, Jan. 2010, Vol. 150, No 1-4, pp.81-124.

[4] National Academies of Sciences, Engineering, and Medicine. 2016. NASA Space Technology Roadmaps and Priorities Revisited. Washington, DC: *The National Academies Press*. doi: 10.17226/23582.

[5] National Academies of Sciences, Engineering, and Medicine. 2016. Achieving Science with CubeSats: Thinking Inside the Box. Washington, DC: *The National Academies Press*.

[6] H. Kalita, J. Thangavelautham, "Automated Multidisciplinary Design and Control of Hopping Robots for Exploration of Extreme Environments on the Moon and Mars," *70th International Astronautical Congress (IAC)*, Washington D.C., USA, 2019, 21-25 October.

[7] H. Kalita, A. S. Gholap, J. Thangavelautham, "Dynamics and Control of a Hopping Robot for Extreme Environment Exploration on the Moon and Mars," *IEEE Aerospace Conference*, Big Sky, USA, 2020, 7-14 March.

[8] H. Kalita, T. M. Jameson, G. Stancu, J. Thangavelautham, "Design and Analysis of a Mechanical Hopping Mechanism Suited for Exploring Low-gravity Environments," *IEEE Aerospace Conference*, Big Sky, USA, 2020.

[9] J. Thangavelautham, M. S. Robinson, A. Taits, et al., "Flying, hopping Pit-Bots for cave and lava tube exploration on the Moon and Mars" *2nd International Workshop on Instrumentation for Planetary Missions*, NASA Goddard, 2014.

[10] H. Kalita, A. Ravindran, S. Morad, J. Thangavelautham, "Path Planning and Navigation Inside Off-World Lava Tubes and Caves," *IEEE/ION PLANS Conference*, 2018.

[11] H. Kalita, J. Thangavelautham, "Multirobot Cliff Climbing on Low-Gravity Environments," *11th NASA/ESA Conference on Adaptive Hardware and Systems*, Pasadena, USA, 2017, 24-27 July.

[12] J. Larminie and A. Dicks, "Fuel Cell Systems Explained," Wiley, 2003.

[13] H. Kalita, J. Thangavelautham, "Lunar CubeSat Lander to Explore Mare Tranquilitatis Pit," *AIAA SciTech Forum*, Orlando, USA, 2020.